



Trans. Nonferrous Met. Soc. China 33(2023) 2843–2852

Transactions of Nonferrous Metals Society of China

www.tnmsc.cn



Impurity distribution in preparation of high-purity aluminum by vacuum zone melting

Meng-ping DUAN^{1,2,3,4}, Jin-yang ZHAO^{1,2,3,4}, Bao-qiang XU^{1,2,3}, Ling-xin KONG^{1,2,3,4}, Bin YANG^{1,2,3,4}, He-li WAN^{1,2,3,4}, Cheng-cheng FU²

- 1. National Engineering Research Center of Vacuum Metallurgy, Kunming University of Science and Technology, Kunming 650093, China;
 - 2. Faculty of Metallurgical and Energy Engineering, Kunming University of Science and Technology, Kunming 650093, China;
- 3. Key Laboratory for Vacuum Metallurgy of Non-ferrous Metals of Yunnan Province, Kunming 650093, China;
- 4. State Key Laboratory of Nonferrous Metal Resources Clean Utilization in Yunnan Province, Kunming 650093, China

Received 29 March 2022; accepted 14 July 2022

Abstract: A novel vacuum zone melting process for preparing high-purity Al was proposed. The axial segregation of impurities was investigated by determining the equilibrium distribution coefficient. Theoretical and experimental results showed that impurities (Cu, Si, and Fe) with an equilibrium distribution coefficient k_0 <1 accumulated in the tail of the Al ingot, while Ti (k_0 >1) accumulated at the head end of the ingot. When the molten area moving at 1.5 mm/min and zone melting was performed 15 times, the removal rate of the impurities and the purity of Al were the highest. In the middle of the Al ingot, i.e. 140 mm away from the head end of the sample, the removal rates of Cu, Fe, and Si were higher than 90%, that of Ti was higher than 75%, and the Al content was higher than 99.999%. The purity of the Al samples met the requirements of the commercial 99.999% (5N) high-purity Al standard.

Key words: vacuum zone melting; high-purity Al; equilibrium distribution coefficient; impurity purification

1 Introduction

As a basic material, high-purity Al exhibits higher conductivity, thermal conductivity, corrosion resistance, and lower magnetic conductivity than raw Al, and is widely used to prepare electrolytic capacitors and metals or alloys for aerospace applications [1]. With the rapid development of the aerospace industry, the domestic demand for high-purity Al is also increasing. The State Council issued the comprehensive work plan for energy conservation and emission reduction in the 14th Five Year Plan, which pointed out that it is

necessary to further improve the policy mechanism for energy conservation and emission reduction, promote the substantial improvement of energy utilization efficiency and the continuous reduction of the total emission of major pollutants. Therefore, it is necessary to identify a clean and efficient method to prepare high-purity Al.

The zone melting method was invented by PFANN [2] in the middle of the 20th century. It was originally used to purify germanium. This method has evolved over the last 60 years, and has been widely used to prepare high-purity metals and some rare-earth metals [3–5]. Moreover, the zone melting method offers economic and environmental

advantages because it is solely a physical purification method. Zone melting is also the primary method used presently for preparing ultra-high-purity Al [6].

The distribution characteristics of impurities and the microstructures of Al are determined by the temperature distribution and travel speed of the molten area during zone melting process [7,8]. Therefore, the heat transfer characteristics merit further study. Some researchers [9,10] have focused on the simulation of the purification process, and a few experimental studies have focused on the preparation of high-purity Al by zone melting [11]. CHEUNG et al [12] conducted simulations using a numerical model capable of predicting the solute redistribution at any stage in the melting step of multi-pass zone melting, and found that the optimization of the zone melting of Al was affected by a variable k (termed the "distribution coefficient"). However, that study only compared the simulation and experimental results under the same experimental conditions, and did not report the migration and distribution of impurities at different zone melting times and different travel speeds of the molten area. WANG et al [13] used code to obtain analytical solutions via a data transfer from global modeling. The simulation results indicated that the Marangoni convection and forced convection of the crystal rotation purification efficiency of crystal rotation is indistinctive in the zone remelting purification process. Additionally, SPIM et al [14] simulated the zone melting of aluminum using a simulation model that simulated the distribution of impurities with different melting zone widths and travel speeds.

In this study, the migration and distribution behaviors of impurities at different zone melting times and travel speeds of the molten area were investigated under vacuum conditions. Impurities (Cu, Si, and Fe) with an equilibrium distribution coefficient of $k_0 < 1$ accumulated in the tail of the Al ingot, while Ti ($k_0 > 1$) accumulated at the head end of the ingot, and 5N Al was prepared. The purification of Al under vacuum conditions can facilitate the volatilization of some impurities, prevent contamination by impurities, and prevent the loss of heat by the inert gas. This study provides experimental data and guidance for the preparation of high-purity Al by vacuum zone melting.

2 Experimental

2.1 Materials and procedure

The raw Al sample was a cuboid (length L=40 mm, width W=17 mm, and height H=15 mm), in which the impurity content was uniform. To avoid contamination from the material surface, during the experiment, the sample surface was polished in a mixed solution of ethanol and hydrochloric acid, then rinsed with ethanol, and placed in a graphite boat (L=300 mm, W=20 mm, and H=20 mm). The graphite boat was placed in a transparent quartz tube, and then heated using a magnetic induction heating coil. The graphite boat conducted heat to the Al ingot to realize the melting and flow of the ingot. The experimental apparatus is shown in Fig. 1; the content of each impurity element in the raw material is listed in Table 1.

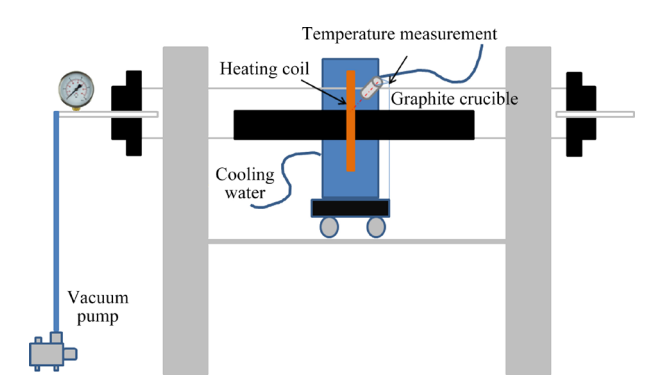


Fig. 1 Schematic of zone melting furnace

* wt.%

Table 1 Composition of raw materials used in experiments (mg/kg)

Al*	Cu	S	Si	Fe	Ti
99.9948	8 9.343	4 8.9	569	6.3435	1.2628
Se	Cl	P	S	Mg	Others
2.1	1.9269	6.3172	3.5452	2 8.4	3.8035

At the beginning of the experiment, the magnetic induction heating coil was fixed at 40 mm from the right end of the crucible to ensure the stability of the temperature field during the experiment. When the system pressure was reduced to $5\times10^{-1}\,\mathrm{Pa}$, the power of the zone melting furnace was slowly adjusted to 2 kW. Subsequently, the power was increased to 5 kW after increasing the temperature to 450 °C. The magnetic induction

heating coil was slowly moved from the right to the left after the Al ingot melted at 680 °C. The heating and coil movement were stopped when the coil was 40 mm from the left end. The coil was then returned to the starting position to begin the next run of melting after decreasing the temperature to 25 °C. The product was subsequently removed for component analysis after the completion of purification.

2.2 Chemical analysis

The purified Al sample was cut by wire cutting; the length of the cut sample was 40 mm, which was the same as the width of the molten area. Subsequently, the surface of the segmented sample was sequentially cleaned using a 20% NaOH solution, deionized water, and alcohol, and polished. Finally, glow discharge mass spectrometry (GDMS, Element GD) was employed to analyze the main impurity content in the purified sample. The composition of the samples at different positions was analyzed. Figure 2 shows the sample analysis procedure.



Fig. 2 Schematic of sample analysis procedure

Figure 3 shows a schematic identifying the analysis points on the samples. The principle of GDMS is to use the measured sample with flat surface as the cathode of glow discharge, the sample produces cathode sputtering in DC or RF or pulse glow discharge device, and the sputtered sample atoms leave the sample surface and diffuse into the plasma [15,16]. Through the mass-to-charge ratio of each element and the strength of the response signal, qualitative and quantitative analysis of the element to be analyzed was carried out [17]. A high-purity Al standard sample was used to calibrate the GDMS parameters so as to ensure accuracy of the test results. Relative Standard Deviation (RSD) was employed to analyze the analysis precision of the results. The value of RSD

was obtained by dividing the standard deviation by the corresponding average value multiplied by 100%. The value of RSD was in the range from 1% to 10% in this work.

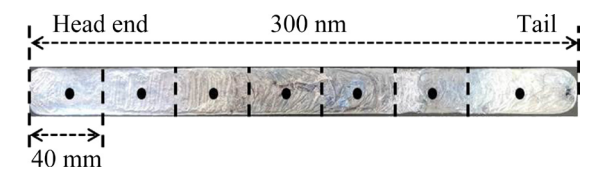


Fig. 3 Analysis points of samples

3 Results and discussion

3.1 Theoretical analysis

Zone melting separates impurities generated during continuous local melting and solidification by utilizing different solubilities of the impurities in the solid-liquid phase of the main metal [18,19]. When the metal is melted in a high-purity graphite crucible, a part of the material in the crucible is in a state of solid-liquid coexistence [20,21]. The solubilities C_s and C_l of different impurities in the solid-liquid phase are different, and the ratio of $C_{\rm s}$ to C_1 is defined as the equilibrium distribution coefficient, k_0 [22–24]. However, in the experiment, the equilibrium distribution coefficient is not only determined by the solubility of impurities between solid and liquid, but also affected by the moving rate of molten zone and the thickness of boundary layer, which is called effective distribution coefficient (k_{eff}). The relationship between k_{eff} and k_0 can be expressed as

$$k_{\text{eff}} = \frac{k_0}{k_0 + (1 - k_0) \exp(-v\delta/D)}.$$

where D is the impurity diffusivity in the melt, δ is the thickness of the diffusion layer adjacent to the solidification interface (outside this, convection is assumed to produce a uniform liquid composition), and v is the travel speed of the molten area. k_0 is assumed as a non-variable in this study. The main impurities in Al and the value of k_0 are shown in Table 2.

Table 2 Equilibrium distribution coefficients of some impurities in aluminum

Impurity	Cu	Si	Fe	Ti
$\overline{k_0}$	0.140	0.100	0.023	9.800

Impurity elements with $k_0 < 1$ are concentrated in the liquid phase of Al and can be removed by zone melting. If the molten zone moves slowly from the left to the right, impurities with $k_0 < 1$ will gradually move to the right along with the molten zone, and finally accumulate at the end of the sample, as shown in Fig. 4.

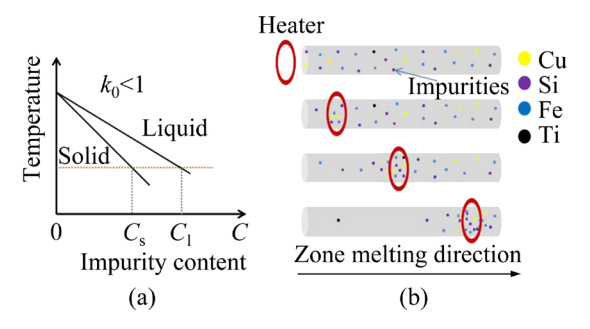


Fig. 4 Relationship between impurity content and temperature in solid and liquid phases (a) and schematic showing zone melting and impurity migration (b)

3.2 Effect of travel speed of molten area

The main impurity requirements to meet the commercial 5N high-purity Al standard are listed in Table 3.

Table 3 Impurity content standard of 5N aluminum

Impurity	Cu	Si	Fe	Ti
Content/(mg·kg ⁻¹)	0.5	1.0	1.0	0.5

The effects of the travel speed of the molten area on the impurity distribution were investigated based on the impurity content in the raw materials. Figure 5 shows the impurity distribution after 15 times of zone melting under different travel speeds of the molten area. The contents of Cu, Si, and Fe in the sample gradually increase along the axial direction of the ingot. They are significantly influenced by k_0 , and the values of which are 0.14, 0.1, and 0.023 for Cu, Si, and Fe, respectively.

Figures 5(a) and (b) show that the impurities Cu and Si are transferred with the molten area and enriched in the sample tail (220 mm from the head end); this phenomenon is significantly affected by the travel speed of the molten area. The impurity content in the same part significantly decreases when the travel speed decreases from 4.6 to 0.7 mm/min. The impurity contents at 140 mm from the head end of the sample are the lowest. The contents of Cu and Si in the sample at this location

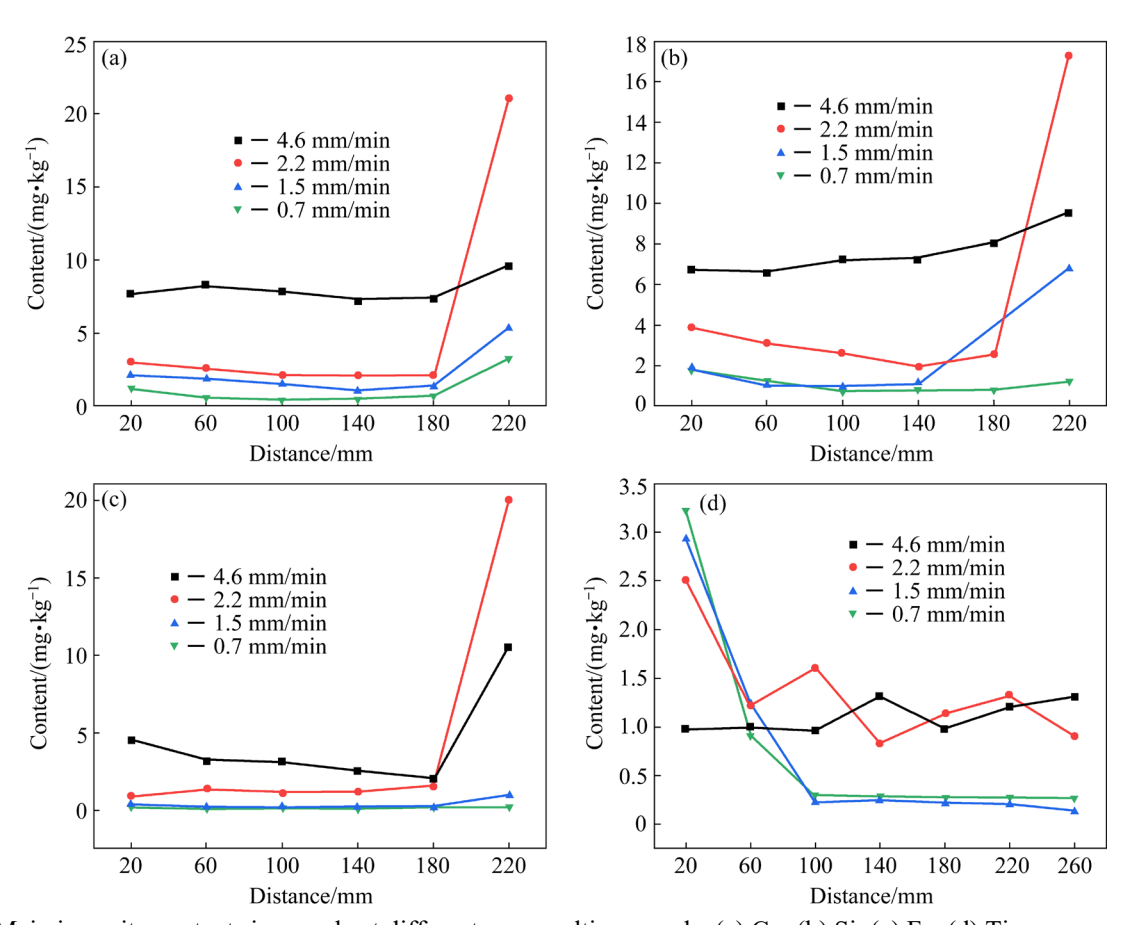


Fig. 5 Main impurity contents in sample at different zone melting speeds: (a) Cu; (b) Si; (c) Fe; (d) Ti

decrease to 0.9281 and 1.1325 mg/kg, respectively, at a travel speed of 1.5 mm/min, and 0.5334 and 0.7968 mg/kg, respectively, at a travel speed of 0.7 mm/min. The composition curves of Cu and Si at these two travel speeds almost coincide. This result shows that after 15 times of zone melting at 1.5 mm/min, the migration of impurities reaches equilibrium, a continuous reduction in the travel speed has little effect on the purification, and very low travel speeds will increase the energy and labor costs.

Figure 5(c) shows the content distribution of Fe at different locations in the sample. As the k_0 of Fe is very small (0.023), the solubility of Fe in the liquid state is higher, making it the easiest to transfer with the molten area. Figure 5(c) shows that the Fe content in the middle is lower than at the head end and tail, and a large amount of Fe is concentrated in the tail of the Al ingot. The minimum impurity content of Fe is 0.1075 mg/kg (at 140 mm from the head end) when the travel speed of the molten area is 0.7 mm/min. With a similar trend as before, the Fe content in the sample decreases with decreasing travel speed. However, the difference in the content of Fe in the sample is negligible when the travel speed changes from 1.5 to 0.7 mm/min.

Ti is an impurity with $k_0 > 1$, and its migration law is opposite to that for $k_0 < 1$. Figure 5(d) shows that Ti is enriched at the head end of the sample. The impurity content of Ti in the head end of the sample inecreases gradually with a decrease in the travel speed of the molten area. When the travel speed decreases to 2.2 mm/min and lower, the migration trend of Ti is distinct, and its content at the head end increases gradually. The extent of increase in the impurity content of Ti is lower at the head end, and its value in other parts does not continue to decrease with a decrease in the travel speed of the molten area to 1.5 mm/min, indicating that the migration of Ti reaches equilibrium at this speed and with 15 times of zone melting. The experimental results show that the travel speed of the molten area should ideally be low to improve the refining efficiency for different impurity elements ($k_0 < 1 \text{ or } k_0 > 1$).

The equilibrium data for the Al content obtained from four groups of experiments are plotted in Fig. 6 to intuitively analyze the change in the Al content in each part. No standard high-purity

Al ingot was obtained at a travel speed of 4.6 mm/min; therefore, this data set was discarded and the other three data sets were analyzed. Figure 6 shows that the content of Al gradually increases at the same position when the zone melting speed is reduced from 2.2 to 0.7 mm/min. There is a concurrent increase in the number of samples meeting the purity requirements of 5N Al from three pieces at 2.2 mm/min to six pieces at 0.7 mm/min. Figure 6 also shows that the highest Al content is obtained at 100-180 mm from the head end (Fig. 3) in each set of the test results; this position, corresponds to the middle of the ingot. This is because the impurity content for $k_0 < 1$ and $k_0 > 1$ in the middle of the ingot is the lowest among the values for the entire product; consequently, the purity of Al is the highest.

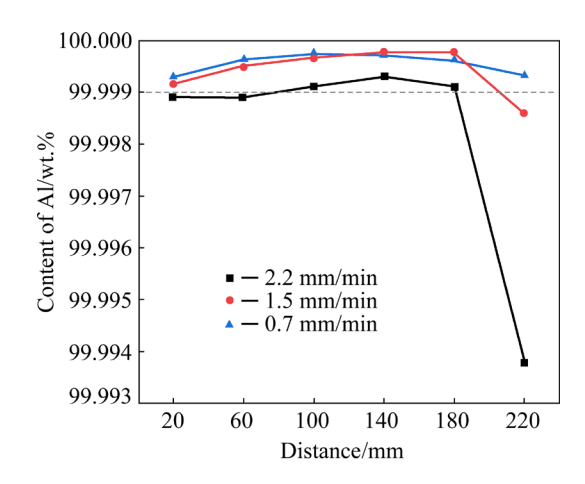


Fig. 6 Effect of travel speed of molten area on content of Al

The results for the middle of the ingot, which had an Al content of 99.9997%, were obtained when the travel speed of the molten area was 1.5 mm/min, and were the same as those obtained at 0.7 mm/min, which indicates that the impurities fully migrated to the tail when the travel speed was 1.5 mm/min and 15 times of zone melting were conducted.

Figure 7 shows that the removal rates of the Cu, Si, Fe, and Ti impurities increase with a decrease in the travel speed of the molten area. The increase in the removal rates of the impurities is small when the travel speed is decreased from 1.5 to 0.7 mm/min, which indicates that the impurity migration reaches equilibrium after 15 times of zone melting at 1.5 mm/min. The removal rates of elements with $k_0 < 1$, such as Cu, Si, and Fe, are

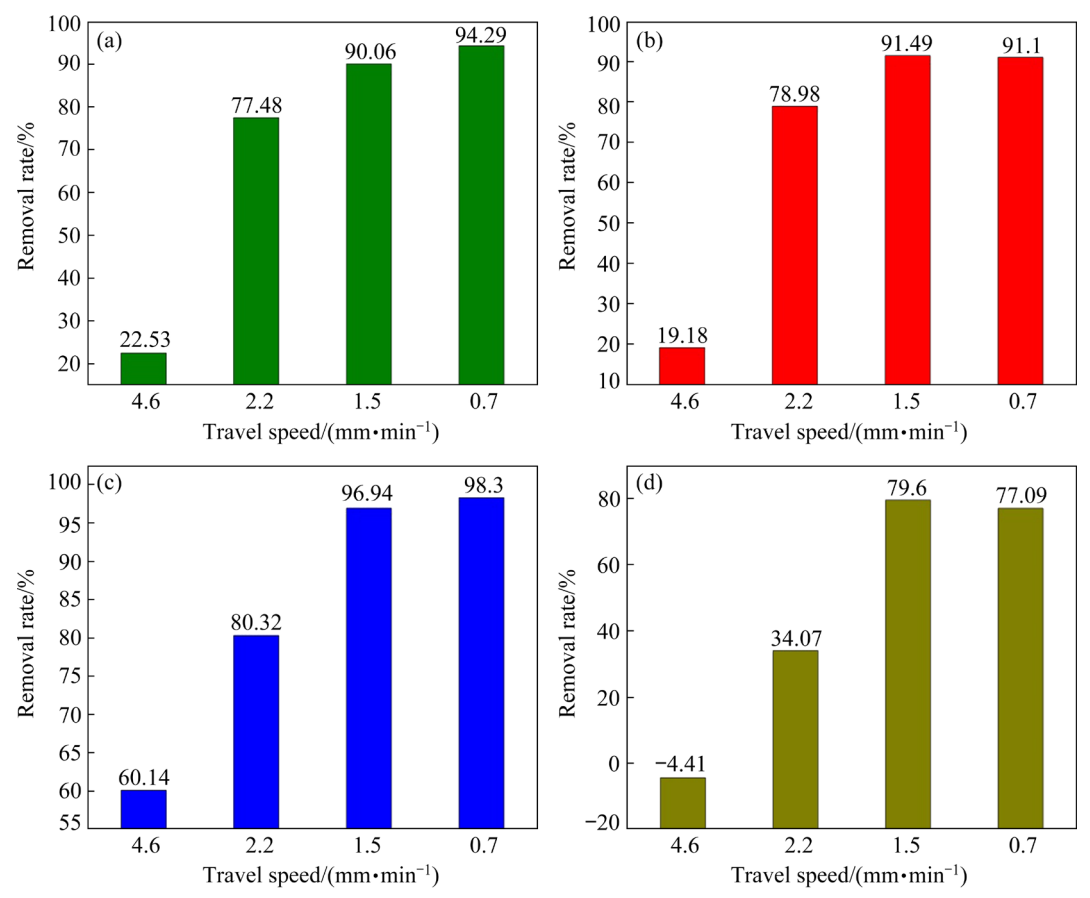


Fig. 7 Dependence of removal rate of impurities on travel speed of molten area: (a) Cu; (b) Si; (c) Fe; (d) Ti

higher than 90% when the travel speed of the molten area is decreased to 1.5 mm/min. Figure 7(d) shows the dependence of the removal rate of the Ti impurity on the travel speed of the molten area. The removal rate of Ti is -4.41% when the travel speed is 4.6 mm/min, indicating that Ti migrates slowly and its distribution in the product is irregular, resulting in a content higher than that in the raw material. When the travel speed is decreased to 2.2 mm/min, the removal rate is 34.07%, indicating that Ti has begun to migrate to the head end. The removal rate of Ti increases from 34.07% to 79.6% when the travel speed is decreased from 2.2 to 1.5 mm/min. However, the removal rate decreases when the travel speed is decreased to 0.7 mm/min, indicating that the distribution equilibrium of Ti has been reached at 1.5 mm/min. The above results show that the removal rate of impurities is the best and the purity of Al is the highest when the travel speed of the molten area is 1.5 mm/min.

3.3 Effect of zone melting times

Figure 8 shows the dependence of the content distributions of Cu, Si, Fe, and Ti impurities on the

zone melting times at a travel speed of 1.5 mm/min of the molten area.

Figure 8(a) shows that the content of the Cu impurity at the tail of the sample increases with increasing zone melting times. At 140 mm from the head end of the sample, it decreases from 5.0726 to 0.9281 mg/kg, and the distribution is more uniform when the number of melting times is increased from 5 to 15. Similarly, the content of the Si impurity in the tail increases with increasing melting times, and at 140 mm from the head end of the sample, it decreases from 6.8627 to 1.1325 mg/kg when the number of melting times is increased from 5 to 15 (Fig. 8(b)). The Fe impurity only accumulates at the tail, and its content is less than 1 mg/kg when the number of melting time is 15, which meets the requirements of the impurity content of 5N Al.

The migration trend of Ti in the Al ingot is opposite to that of the impurities with $k_0 < 1$, as shown in Fig. 8(d). When the number of zone melting times is 5, Ti is almost evenly distributed in the Al melt and there is no distinct migration. When the number of times is increased to 10, the Ti content at the head end of the sample is higher than

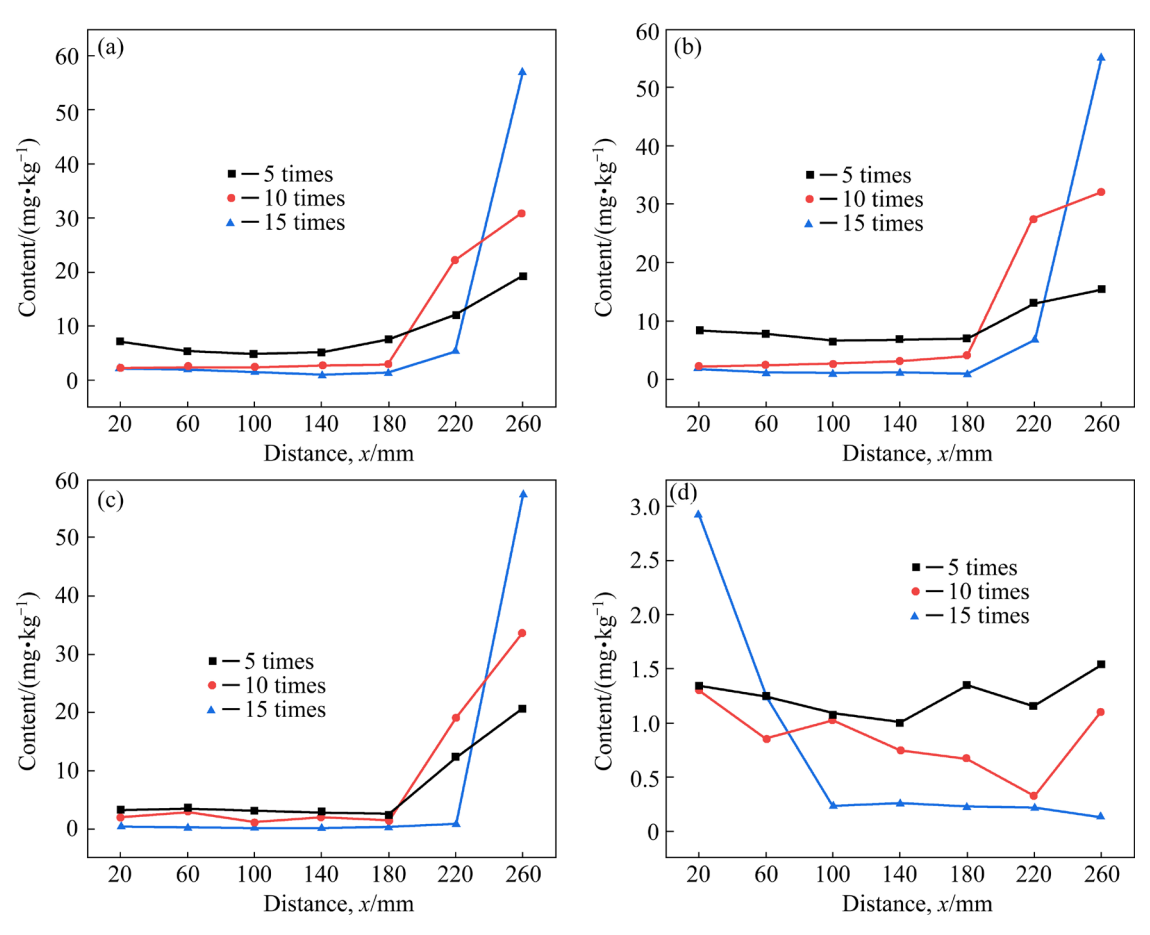


Fig. 8 Dependence of content of impurities on zone melting times at travel speed of molten area of 1.5 mm/min: (a) Cu; (b) Si; (c) Fe; (d) Ti

that in other places, indicating that Ti has begun to migrate to the head end. Ti exhibits pronounced migration and accumulates at the head end after zone melting for 15 times, which indicates that Ti can be removed well after 15 times of zone melting under vacuum.

Figure 9 shows the relationship between the Al content in various parts of the product and number of times of zone melting. The Al content in the same position of the product increases with a gradual increase in the number of zone melting times when the travel speed of the molten area is 1.5 mm/min. Under the same number of zone melting times, at distance from 20 to 180 mm of the head end, the Al content gradually increases and then decreases, and is the highest between 140 and 180 mm from the head end of the sample. The Al content is the highest (99.99974%) at 140 mm from the head end after 15 times of zone melting. This result shows that the impurity removal effect is significantly enhanced with an increase in the number of times of zone melting.

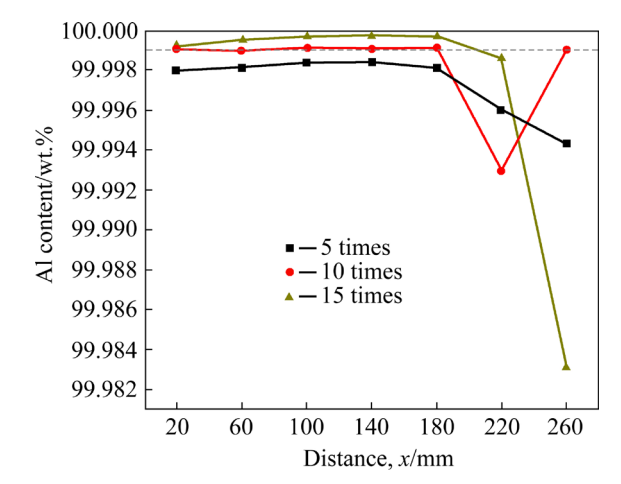


Fig. 9 Relationship between Al content and zone melting times

Figure 10 shows the relationship between the removal rates of the Cu, Si, Fe, and Ti impurities calculated based on the impurity content at 140 mm from the head end and the number of zone melting times. The removal rates of the impurities gradually increase with an increase in the number of melting

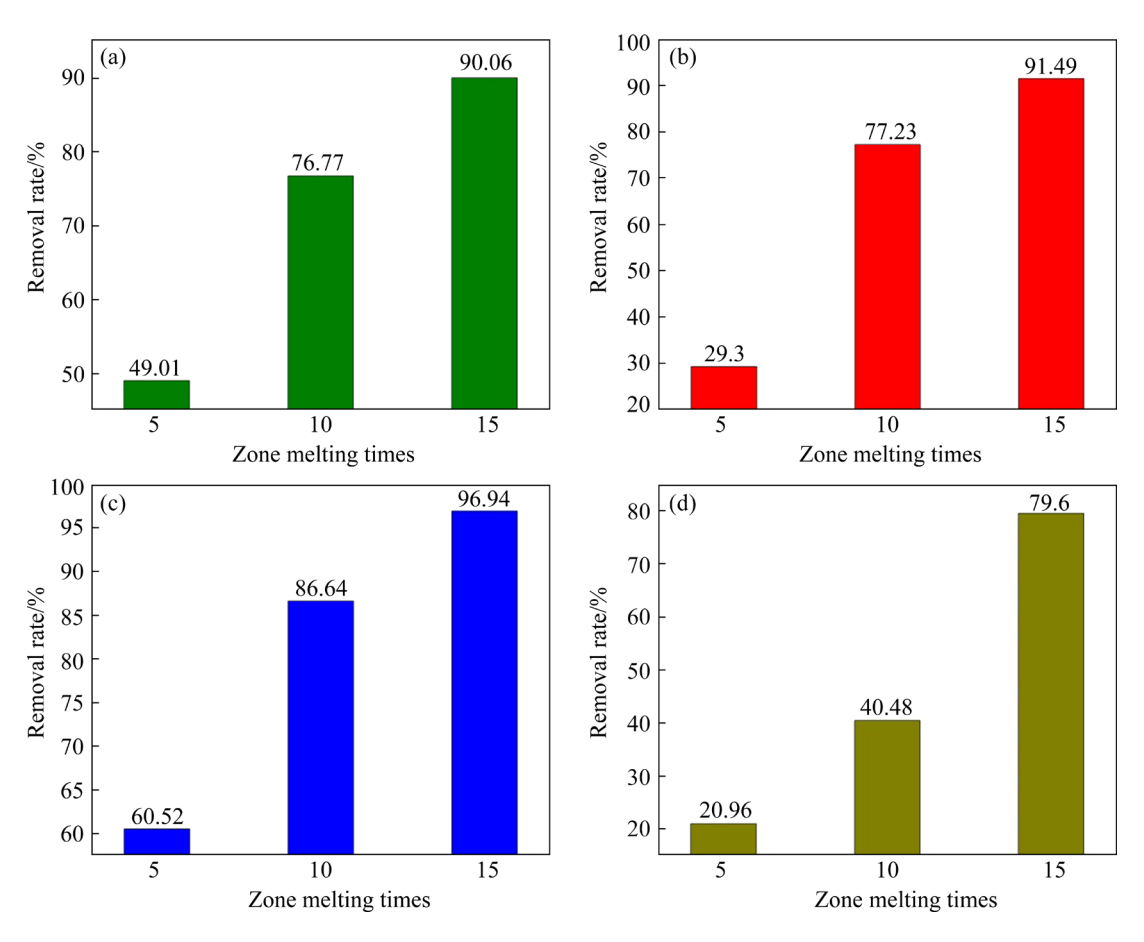


Fig. 10 Dependence of removal rate of impurities on zone melting times at travel speed of 1.5 mm/min: (a) Cu; (b) Si; (c) Fe; (d) Ti

times. The removal rates of three impurity elements, Cu, Si, and Fe with $k_0 < 1$, are higher than 90% after 15 times of zone melting, and the removal rate of Fe is the highest (96.94%) because its k_0 is the smallest. The removal rate of Ti with $k_0 > 1$ is low after 5 times of zone melting, and it is increased from 40.48% to 79.6% when the number of zone melting times is increased from 10 to 15. Figure 10 also shows that the removal rate of impurities with $k_0 > 1$ is lower than that of impurities with $k_0 < 1$, which indicates that Ti is difficult to remove compared to other impurities.

4 Conclusions

(1) Cu, Si, and Fe, with $k_0 < 1$, migrated and accumulated at the head end of the samples. The purification effect was enhanced with decreasing the travel speed of the molten area and increasing the number of zone melting times. The removal rates of Cu, Fe, and Si were higher than 90%, and their contents in the middle of the sample (i.e.,

140 mm from the head end) were 0.9281, 1.1325, and 0.1075 mg/kg, respectively. The Al content was higher than 99.999% when the travel speed of the molten area was 1.5 mm/min and the number of zone melting times was 15.

- (2) Ti with $k_0 > 1$ accumulated at the head end of the sample. The removal effect was enhanced with decreasing the travel speed of the molten area and increasing the number of zone melting times. The removal rate of Ti was higher that 75%, and its content was 0.1324 mg/kg when the travel speed of the molten area was 1.5 mm/min and the number of zone melting times was 15.
- (3) This study provides reliable experimental data for the purification of Al and other metals using vacuum zone melting, and provides guidance for the improvement of the zone melting method.

Acknowledgments

This work was financially supported by the National Natural Science Foundation of China (No. 51734006), the Outstanding Youth Project of

Yunnan Province, China (No. 202001AV070002), and the Fundamental Research Project of Yunnan Province, China (No. 2019FD037).

References

- CURTOLO D C, XIONG N, FRIEDRICH S, FRIEDRICH B. High and ultra-high-purity aluminum: A review on technical production methodologies [J]. Metals, 2021, 11(9): 1407.
- [2] PFANN W G. Zone melting [J]. Metallurgical Reviews, 1957, 2(1): 29–76.
- [3] CURTOLO D C, FRIEDRICH S, FRIEDRICH B. High purity germanium: A review on principle theories and technical production methodologies [J]. Journal of Crystallization Process and Technology, 2017, 7(4): 65–84.
- [4] ZAIOUR A, ZAHRAMAN K, ROUMIE M, CHARARA J, FAWAZ A, LMAI F, HAGE-ALI M. Purification of tellurium to nearly 7N purity [J]. Materials Science and Engineering: B, 2006, 131(1/2/3): 54-61.
- [5] MUNIRATHNAM N R, PRASAD D S, SUDHEER C H, RAO J V, PRAKASH T L. Zone refining of cadmium and related characterization [J]. Bulletin of Materials Science, 2005, 28(3): 209–212.
- [6] CAO P. Comparison and analysis of the preparation methods of high purity aluminum [J]. World Nonferrous Metals, 2018(11): 10–11. (in Chinese)
- [7] WAN H L, ZHAO J Y, YANG B, XU B Q, DUAN M P, KONG L X, DAI Y N. Study on the effective distribution coefficient of impurity separation in the preparation of high purity aluminum [J]. Journal of Materials Research and Technology, 2020, 9(5): 10366–10376.
- [8] WAN H, KONG L, YANG B, XU B, DUAN M, DAI Y. Zone melting under vacuum purification method for high-purity aluminum [J]. Journal of Materials Research and Technology, 2022, 17: 802–808.
- [9] HASHIMOTO E, UEDA Y, KINO T. Purification of ultra-high purity aluminum [J]. Le Journal de Physique IV, 1995, 5(C7): 153–157.
- [10] CHEUNG T, CHEUNG N, TOBAR C M T, CARAM R, GARCIA A. Application of a genetic algorithm to optimize purification in the zone refining process [J]. Materials and Manufacturing Processes, 2011, 26(3): 493–500.
- [11] CHEUNG T, CHEUNG N, GARCIA A. Application of an artificial intelligence technique to improve purification in the zone refining process [J]. Journal of Electronic Materials, 2010, 39(1): 49–55.
- [12] CHEUNG N, BERTAZZOLI R, GARCIA A. Experimental impurity segregation and numerical analysis based on variable solute distribution coefficients during multi-pass

- zone refining of aluminum [J]. Journal of Crystal Growth, 2008, 310(6): 1274–1280.
- [13] WANG S, FANG H S, JIN Z L, ZHAO C J, ZHENG L L. Integrated analysis and design optimization of germanium purification process using zone-refining technique [J]. Journal of Crystal Growth, 2014, 408: 42–48.
- [14] SPIM J A Jr, BERNADOU M J S, GARCIA A. Numerical modeling and optimization of zone refining [J]. Journal of Alloys and Compounds, 2000, 298(1/2): 299–305.
- [15] BOGAERTS A, GIJBELS R. New developments and applications in GDMS [J]. Fresenius' Journal of Analytical Chemistry, 1999, 364(5): 367–375.
- [16] DOUTHITT C B. Commercial development of HR-ICPMS, MC-ICPMS and HR-GDMS [J]. Journal of Analytical Atomic Spectrometry, 2008, 23(5): 685–689.
- [17] JAKUBOWSKI N, FELDMANN I, STUEWER D. Comparison of ICP-MS with spark ablation and GDMS for direct element analysis of conductive solids [J]. Spectrochimica Acta (Part B): Atomic Spectroscopy, 1995, 50(4/5/6/7): 639-654.
- [18] CHEUNG N, BERTAZZOLI R, GARCIA A. Numerical and experimental analysis of an approach based on variable solute distribution coefficients during purification by zone refining [J]. Separation and Purification Technology, 2007, 52(3): 504–511.
- [19] ZHANG X X, FRIEDRICH S, FRIEDRICH B. Production of high purity metals: a review on zone refining process [J]. Journal of Crystallization Process and Technology, 2018, 08(1): 33-55.
- [20] XU J, ZHU X C, SHAN D B, GUO B, LANGDON T G. Effect of grain size and specimen dimensions on micro-forming of high purity aluminum [J]. Materials Science and Engineering: A, 2015, 646: 207–217.
- [21] KIM P, MIHARA Y, OZAWA E, NOZAWA Y, HAYASHI C. High purity metal production using dry refining processes [J]. Materials Transactions, JIM, 2000, 41(1): 37–43.
- [22] AVAZKONANDEH-GHARAVOL M H, HADDAD-SABZEVAR M, FREDRIKSSON H. Effect of partition coefficient on microsegregation during solidification of aluminum alloys [J]. International Journal of Minerals, Metallurgy, and Materials, 2014, 21(10): 980–989.
- [23] LI M X, TIAN Q L, WU M Z, PENG J B, ZHANG J T, CHEN L S, LU X W, XU Z S, ZHENG H X. Numerical simulation analysis on solute redistribution of In–1wt.%Sn alloy during multipass vertical zone refining process [J]. Journal of Crystal Growth, 2021, 565: 126156.
- [24] DOST S, LIU Y C, HAAS J, ROSZMANN J, GRENIER S, AUDET N. Effect of applied electric current on impurity transport in zone refining [J]. Journal of Crystal Growth, 2007, 307(1): 211–218.

真空区域熔炼法制备高纯铝过程中杂质的分布

段梦平 1,2,3,4, 赵晋阳 1,2,3,4, 徐宝强 1,2,3, 孔令鑫 1,2,3,4, 杨 斌 1,2,3,4, 万贺利 1,2,3,4, 付程程 2

- 1. 昆明理工大学 真空冶金国家工程研究中心, 昆明 650093;
 - 2. 昆明理工大学 冶金与能源工程学院, 昆明 650093;
 - 3. 云南省有色金属真空冶金重点实验室, 昆明 650093;
- 4. 云南省有色金属资源清洁利用国家重点实验室,昆明 650093

摘 要:提出一种真空区域熔炼法制备高纯铝的新工艺。通过确定平衡分配系数,研究杂质的轴向偏析。理论分析和实验结果表明,平衡分配系数 $k_0<1$ 的杂质(Cu、Si 和 Fe)在铝锭尾部累积,而 Ti $(k_0>1)$ 在铝锭首端累积。当熔区以 1.5 mm/min 的速度移动并进行 15 次区域熔炼后,杂质的去除率和铝的纯度最高。在铝锭中部,即距铝样首端 140 mm 处,铜、铁和硅的去除率均高于 90%,钛的去除率高于 75%,铝纯度高于 99.999%。铝样品的纯度符合 99.999% (5N)工业用高纯铝标准的要求。

关键词: 真空区域熔炼; 高纯铝; 平衡分配系数; 杂质净化

(Edited by Wei-ping CHEN)